

Testing of quasi-elastic neutrino charged-current and two-body meson exchange current models with the MiniBooNE neutrino data and analysis of these processes at energies available at the NOvA experiment

A. V. Butkevich¹ and S. V. Luchuk^{1,2}

¹*Institute for Nuclear Research, Russian Academy of Sciences, Moscow 117312, Russia*

²*Moscow Institute of Physics and Technology, Dolgoprudny 141701, Russia*

(Dated: December 31, 2018)

The charged-current quasi-elastic (CCQE) scattering of muon neutrinos on a carbon target is analyzed using the relativistic distorted-wave impulse approximation (RDWIA) taking into account the contribution of the two-particle and two-hole meson exchange current ($2p - 2h$ MEC) to the weak response functions. A fit the RDWIA+MEC model to the MiniBooNE neutrino data is performed and the best fit value of nucleon axial mass $M_A = 1.2 \pm 0.06$ GeV is obtained. We also extract the values of the axial form factor $F_A(Q^2)$ as a function of the squared momentum transfer Q^2 from the measured $d\sigma/dQ^2$ cross section. The flux-integrated CCQE-like differential cross sections for neutrino scattering at energies of the NOvA experiment are estimated within the RDWIA+MEC approach .

PACS numbers: 25.30.-c, 25.30.Bf, 25.30.Pt, 13.15.+g

I. INTRODUCTION

The high-intensity muon-(anti)neutrino beams used in long-baseline neutrino oscillation experiments are peaked in the energy range from a few hundreds of MeV to several GeV. In this energy regime the dominant contribution to neutrino-nucleus scattering comes from the charged-current quasielastic (CCQE) interaction, two-body meson exchange current (MEC), and resonance production processes. To determine values of neutrino oscillation parameters, the probabilities of ν_μ disappearance and ν_e appearance versus neutrino energy are measured in these experiments. The accuracy of these measurements depends explicitly on how well we

are able to evaluate the energy of the incoming neutrino. This energy can be estimated from the lepton and hadron energies visible in the final state after the neutrino has interacted. Thus the total hadronic deposit is the necessary piece of information for the calorimetric method.

Because the CCQE is a two-body process, the incoming neutrino energy can be calculated using only outgoing lepton kinematics. The measurement of muon momentum and angle allows the estimation of the neutrino energy ε_ν and the squared four-momentum transfer Q^2 . This reconstruction method (kinematic method) works well if the true nature of events were indeed a CCQE process. Nuclear effects, the final state interaction (FSI) between of the outgoing particles and the residual nucleus as well as interactions which are not distinguishable from CCQE in the final state – bias or smear the reconstructed neutrino energy. Therefore a good understanding of these effects is critical.

To model the CCQE scattering from a nuclei, most event generators are based on the relativistic Fermi gas model (RFGM) [1]. In this model the nucleus is described as a system of quasi-free nucleons with a flat momentum distribution up to the same Fermi momentum p_F and nuclear binding energy ϵ_b . With the assumption of the conserved vector current, the only parameter of the weak current which is not well constrained by electron scattering data is the axial nucleon form factor $F_A(Q^2)$. In most analysis of the CCQE interaction, the dipole parametrization of $F_A(Q^2)$ with one parameter, the axial mass M_A is used. Note that dipole parametrization has no strict theoretical basis, and the choice of this parametrization is made by analogy with electromagnetic form factors.

The value of M_A is obtained from a fit to observed Q^2 distribution of events, differential, and total (anti)neutrino CCQE cross sections. Results from global analysis of neutrino-deuterium scattering experiments are very widely spread and the formal averaging of M_A values was done in Ref. [2]: $M_A = 1.026 \pm 0.021$ GeV. This result is also known as the world-averaged value of the axial mass. The NOMAD experiment has reported result on neutrino CCQE scattering on carbon: $M_A = 1.05 \pm 0.02 \pm 0.06$ GeV [3]. The MINERvA experiment [4, 5] has shown good agreement within the RFGM with $M_A \approx 1$ GeV, but requires an enhancement to the transverse response function. A recent reanalysis of the MINERvA flux [6] results in the increases to the normalization of previous cross sections [7, 8] and invalidates conclusions from Refs. [4, 5].

On the other hand the differential cross sections measured by the MiniBooNE collabora-

tion [9–11] can be described within the RFGM only with large value of $M_A = 1.35 \pm 0.017$ GeV. The absolute values of the differential and total cross sections are about 30% larger compared to NOMAD results. Large values of axial mass $M_A \approx 1.1 - 1.3$ GeV have also obtained in other experiments using heavy nuclear targets [12–15].

These results have stimulated many theoretical studies trying to explain the apparent discrepancy between the data and theoretical predictions, and present a considerable challenge to neutrino oscillation experiments. A wide variety of models has been proposed to describe CCQE-like cross sections, identified experimentally as processes in which only a final charged lepton with multinucleon excitations is detected, but the pion absorption contribution is subtracted. The data without subtracting any intrinsic background is called CC0 π . A review of the available CCQE-like cross section models can be found in Refs. [16–18].

Based on the results from different groups it is shown that CCQE-like data are really a combination of the genuine QE and of the two-particle and two-hole meson exchange current ($2p - 2h$ MEC) contributions to weak response functions. Such excitations are induced by two-body currents, hence they go beyond the usual impulse approximation (IA) scheme, in which the probe interacts with only single nucleon and corresponds to the $1p - 1h$ excitations. To describe the genuine QE a model should in principle include the nuclear mean field and nucleon-nucleon (NN) short and long-range correlations in the ground state, as well as final state interaction of the outgoing nucleon with the residual nucleus. More sophisticated descriptions of the CCQE interaction that the RFGM provides are available from a number authors [19–30]. Note that there exist some differences already at level of the genuine quasielastic scattering.

The transverse enhancement effective model to account for MEC effects has been proposed in Ref. [31]. In this model the magnetic form factor for nucleon bound in carbon are modified to describe the enhancement in the electron-carbon QE cross section. An enhancement of the axial nucleon mass in the nonrelativistic continuum random phase approximation has been regarded in Ref. [32]. The contribution of $np - nh$ channel is also taken into account through phenomenological approach in Ref. [33].

The most complete theoretical calculations of $2p - 2h$ cross sections are performed by different groups [34–41]. In Refs. [34–37] the models start from a local Fermi gas picture of the nucleus and take into account long-range random phase approximation (RPA) corrections, but ignore the shell structure of nucleus and FSI effects. In the $2p - 2h$ sector both

models use the Fermi gas approximation. The short-range NN -correlations are included by considering an additional two-body correlation current. As result, the NN -correlations and NN -correlations-MEC-interference naturally appear (RPA-MEC approach).

In the SuSA approach [29, 38–41] a superscaling analysis of electron scattering result is used to calculate neutrino cross sections. The effects of the short-range NN -correlations in the $1p - 1h$ sector are effectively included via the superscaling function. In Ref. [40] the SuSAv2 model is combined with MECs in $2p - 2h$ sector by using accurate parametrizations of the exact calculation of electroweak MEC response functions [38, 39] (SuSAv2-MEC approach). The NN -correlations and NN -correlations-MEC-interference are absent in the $2p - 2h$ MEC contributions.

Another approach which goes beyond the impulse approximation was developed in Ref. [42]. In this work a joint calculation of the CCQE and $2p - 2h$ contributions to the lepton scattering cross sections on carbon, using relativistic distorted-wave impulse approximation (RDWIA) for quasielastic response functions in the electroweak sector (RDWIA+MEC approach) was performed. The RDWIA, which takes into account the nuclear shell structure and final-state interaction effects, was developed to describe of the QE electron-nucleus scattering [43–45]. Results of the analyze data for $^{12}\text{C}(e, e'p)$ based on upon the RDWIA can be found in Refs. [23, 45], which show that the nucleon momentum distributions are described well by mean-field calculations. From this analysis it follows that fragmentation of the $1p$ strength in carbon by collective modes is largely confined to excitation energy be low 10 MeV and approximately 84% of the independent particle shell model (IPSM) is found in the missing energy bin 15-25 MeV. In our approach [22, 23] the effects of the short-range NN -correlations, leading to appearance of a high-momentum and high-energy distribution in the target are estimated.

We explicitly added the MEC contributions (without the NN -correlations-MEC-interference) to the genuine QE interaction, as in the SuSA-MEC approach [40]. The functional forms employed for the parametrizations of the MEC transverse electromagnetic vector response, and for the axial and vector components of the weak response were detailed in Refs. [40, 41]. The RDWIA+MEC approach was successfully tested against $^{12}\text{C}(e, e')$ data [42].

Although theoretical calculations of the CCQE-like neutrino-nucleus cross sections have been performed by many groups using different approaches, at this moment there is no

progress in a quantitative description of the data and it is not clear which models fit the global data best. For example, the global fit performed in Ref. [46] shows very poor results. One of the goals of this paper is to fit the RDWIA+MEC model to the MiniBooNE data [9] for neutrino scattering off carbon. Within this approach we extract the value of the axial mass from measured flux-integrated $d\sigma/Q^2$ and $d^2\sigma/dT d\cos\theta$ (T and θ are, correspondingly, kinetic energy and muon scattering angle) differential cross sections. In addition we determine the values of the axial form factor $F_A(Q^2)$ as a function of Q^2 , using the method described in Ref. [47]. Previously our constraint on the $M_A \approx 1.37$ GeV was obtained within the RDWIA [47, 48]. This work improves the previous situation by including $2p-2h$ MEC contributions. A second topic addressed in this paper is calculations of the CCQE-like flux-integrated differential and double-differential cross sections at energies of the NOvA experiment [49, 50]. We evaluated these cross sections within the RDWIA+MEC approach with value of M_A extracted from the MiniBooNE data.

This article is organized as follows. In Sec. II we briefly present the RDWIA+MEC model and the procedure which allows the determination of values of the axial form factor from the $d\sigma/dQ^2$ differential cross section. Section III presents results of this model to the MiniBooNE data, extraction of the $F_A(Q^2)$, and calculations of the flux-integrated differential cross sections for the NOvA experiment. Our conclusions are summarized in Sec. IV.

II. FORMALISM OF QUASIELASTIC SCATTERING, RDWIA, $2p-2h$ MEC RESPONSES, AND FLUX-INTEGRATED CROSS SECTIONS.

We consider neutrino charged-current QE inclusive

$$\nu_\mu(k_i) + A(p_A) \rightarrow \mu(k_f) + X \quad (1)$$

scattering off nuclei in the one-W-boson exchange approximation. Here $k_i = (\varepsilon_i, \mathbf{k}_i)$ and $k_f = (\varepsilon_f, \mathbf{k}_f)$ are the initial and final lepton momenta, $p_A = (\varepsilon_A, \mathbf{p}_A)$ is the initial target momenta, $q = (\omega, \mathbf{q})$ is the momentum transfer carried by the virtual W-boson, and $Q^2 = -q^2 = \mathbf{q}^2 - \omega^2$ is the W-boson virtuality.

A. CCQE-like quasielastic lepton-nucleus cross sections

In the inclusive reactions (1) only the outgoing lepton is detected and the differential cross sections can be written as

$$\frac{d^3\sigma}{d\varepsilon_f d\Omega_f} = \frac{1}{(2\pi)^2} \frac{|\mathbf{k}_f|}{\varepsilon_i} \frac{G^2 \cos^2 \theta_c}{2} L_{\mu\nu} W^{\mu\nu}, \quad (2)$$

where $\Omega_f = (\theta, \phi)$ is the solid angle for the muon momentum, $G \simeq 1.16639 \times 10^{-11} \text{ MeV}^{-2}$ is the Fermi constant, θ_C is the Cabbibo angle ($\cos \theta_C \approx 0.9749$), $L_{\mu\nu}$ is the lepton tensor, and $W^{\mu\nu}$ are the weak CC nuclear tensors. In terms of response functions the cross sections reduce to

$$\frac{d^3\sigma}{d\varepsilon_f d\Omega_f} = \frac{G^2 \cos^2 \theta_c}{(2\pi)^2} \varepsilon_f |\mathbf{k}_f| (v_0 R_0 + v_T R_T + v_{zz} R_{zz} - v_{0z} R_{0z} - h v_{xy} R_{xy}), \quad (3)$$

where the coupling coefficients v_k , whose expressions are given in [22] are kinematic factors depending on the lepton's kinematics. The response functions are given in terms of components of the hadronic tensors

$$R_0 = W^{00}, \quad (4a)$$

$$R_T = W^{xx} + W^{yy}, \quad (4b)$$

$$R_{0z} = W^{0z} + W^{z0}, \quad (4c)$$

$$R_{zz} = W^{zz}, \quad (4d)$$

$$R_{xy} = i (W^{xy} - W^{yx}) \quad (4e)$$

and depend on the variables (Q^2, ω) or $(|q|, \omega)$.

All the nuclear structure information and final state interaction effects are contained in the weak CC nuclear tensor. It is given by the bilinear products of the transition matrix elements of the nuclear CC operator J_μ^{cc} between the initial nucleus state $|A\rangle$ and the final state $|X_f\rangle$ as

$$W_{\mu\nu} = \sum_f \langle X_f | J_\mu^{(cc)} | A \rangle \langle A | J_\nu^{(cc)\dagger} | X_f \rangle, \quad (5)$$

where the sum is taken over undetected states X_f . This equation includes all possible final states. Thus, the hadron tensor can be expanded as the sum of the $1p - 1h$ and $2p - 2h$, plus additional channels:

$$W^{\mu\nu} = W_{1p1h}^{\mu\nu} + W_{2p2h}^{\mu\nu} + \dots, \quad (6)$$

where the $1p - 1h$ channel gives the CCQE response functions and the $2p - 2h$ hadronic tensor determines the $2p - 2h$ MEC response functions. Thus, the functions R_i (4) can be written as a sum of the CCQE ($R_{i, QE}$) and MEC ($R_{i, MEC}$) response functions

$$R_i = R_{i, QE} + R_{i, MEC}. \quad (7)$$

B. RDWIA model

We describe genuine CCQE neutrino-nuclear scattering in the impulse approximation, assuming that the incoming neutrino interacts with only one nucleon, which is subsequently emitted, while the remaining (A-1) nucleons in the target are spectators. The nuclear current is written as the sum of single-nucleon currents.

The single-nucleon charged current has $V-A$ structure $J^\mu = J_V^\mu + J_A^\mu$. For a free-nucleon vertex function $\Gamma^\mu = \Gamma_V^\mu + \Gamma_A^\mu$ we use the CC2 vector current vertex function $\Gamma_V^\mu = F_V(Q^2)\gamma^\mu + iF_M(Q^2)\sigma^{\mu\nu}q_\nu/2m$, where $\sigma^{\mu\nu} = i[\gamma^\mu, \gamma^\nu]/2$, F_V and F_M are the weak vector form factors. They are related to the corresponding electromagnetic ones for proton and neutron by the hypothesis of the conserved vector current. We use the approximation of Ref. [51] for the vector nucleon form factors. Because the bound nucleons are off-shell we employ the de Forest prescription [52] and use the Coulomb gauge for the off-shell vector current vertex Γ_V^μ .

The axial current vertex function can be written in terms of the axial $F_A(Q^2)$ and pseudoscalar F_P form factors

$$\Gamma_A^\mu = F_A(Q^2)\gamma^\mu\gamma_5 + F_P(Q^2)q^\mu\gamma_5. \quad (8)$$

These form factors are parameterized using a dipole approximation:

$$F_A(Q^2) = \frac{F_A(0)}{(1 + Q^2/M_A^2)^2}, \quad F_P(Q^2) = F_A(Q^2)F'_P(Q^2), \quad (9)$$

where $F'_P = 2m^2/(m_\pi^2 + Q^2)$, $F_A(0) = 1.267$, M_A is the axial mass, and m_π is the pion mass. Then the axial current vertex function can be written in the form

$$\Gamma_A^\mu = F_A(Q^2)[\gamma^\mu\gamma_5 + F'_P(Q^2)q^\mu\gamma_5] \quad (10)$$

and the axial vector current can be factorized as

$$J_A = F_A(Q^2)J'_A(Q^2), \quad (11)$$

where $J'_A = \gamma^\mu \gamma_5 + F'_P(Q^2) q^\mu \gamma_5$

In the RDWIA, the relativistic wave functions of the bound nucleon states are calculated in the IPSM as the self-consistent solutions of a Dirac equation, derived within a relativistic mean field approach, from a Lagrangian containing σ , ω , and ρ mesons (the $\sigma - \omega$ model)[53, 54]. According to the JLab data [45, 55] the occupancy of the independent particle shell model orbitals of ^{12}C equals on average 89%. In this work, we assume that the missing strength (11%) can be attributed to the short-range NN -correlations in the ground state, leading to the appearance of the high-momentum and high-energy component in the nucleon distribution in the target. In the RDWIA, the final state interaction effects for the outgoing nucleon are taken into account. The distorted-wave function of the knocked out nucleon is evaluated as a solution of a Dirac equation containing a phenomenological relativistic optical potential. The EDAD1 parametrization [56] of the relativistic optical potential for carbon was used in this work. We calculated the inclusive cross sections with the EDAD1 relativistic optical potential in which only the real part was included.

The cross sections with the FSI effects in the presence of the short-range NN -correlations were calculated by using the method proposed in Ref. [22] with the nucleon high-momentum distribution from Ref. [57] that was renormalized to value of 11%. In this approach, the contribution of the NN -correlated pairs is evaluated in impulse approximation, *i.e.*, the virtual W-boson couples to only one member of the NN -pair. It is a one-body process that leads to the emission of two nucleons ($2p - 2h$ excitation).

C. $2p - 2h$ excitation

In the present work we evaluate the weak MEC response functions $R_{i,MEC}$ of neutrino scattering on carbon, using accurate parametrizations of the exact MEC calculation [39]. In order to evaluate the $2p - 2h$ hadronic tensor $W_{2p2h}^{\mu\nu}$, in Ref. [39] the RFGM was chosen to describe the nuclear ground state. The short-range NN -correlations and FSI effects were not considered in this approach. The elementary hadronic tensor is given by bilinear product of the matrix elements of the two-body weak (containing vector and axial components) MEC. Only one-pion exchange is included.

The two-body current operator is obtained from the pion production amplitudes for the nucleon while coupling a second nucleon to the emitted pion. The resulting MEC operator

can be written as a sum of seagull, pion-in-flight, pion-pole, and Delta-pole operators. The Δ -peak is the main contribution to the pion production cross section and the MEC peak is located in the “dip” region between the QE and Delta peaks.

The functional forms employed for these parametrizations as functions of $(\omega, |\mathbf{q}|)$ are valid in the range of momentum transfer $|\mathbf{q}| = 200 \div 2000$ MeV. The expressions for the fitting parameters are described in detail in Refs. [40, 41, 58]. Results of lepton-nucleus cross sections obtained using these MEC parametrizations were successfully tested against the experimental world data for ^{12}C [41, 42, 59].

D. Flux integrated cross sections and the method for extraction of $F_A(Q^2)$ from $d\sigma/dQ^2$ distribution.

The inclusive weak hadronic tensor is bilinear in the transition matrix elements of the nuclear weak current operators $W_{\mu\nu} = \langle J_\mu J_\nu^\dagger \rangle$, where the angle brackets denote products of matrix elements appropriately averaged over initial states and summed over final states. By using Eq. (11) the axial vector current can be written as $J = J_V + F_A J'_A$. The expressions for the inclusive CCQE cross sections in terms of vector σ^V , axial σ^A , and vector-axial σ^{VA} cross sections then given by [47]

$$\frac{d\sigma^\nu}{dQ^2}(Q^2, \varepsilon_i) = \sigma^V(Q^2, \varepsilon_i) + F_A^2(Q^2)\sigma^A(Q^2, \varepsilon_i) + hF_A(Q^2)\sigma^{VA}(Q^2, \varepsilon_i) \quad (12a)$$

$$\begin{aligned} \frac{d^2\sigma^\nu}{dT d\cos\theta}(T, \cos\theta, \varepsilon_i) &= \sigma^V(T, \cos\theta, \varepsilon_i) + F_A^2(Q^2)\sigma^A(T, \cos\theta, \varepsilon_i) \\ &+ hF_A(Q^2)\sigma^{VA}(T, \cos\theta, \varepsilon_i), \end{aligned} \quad (12b)$$

where σ^V is the cross section $d\sigma/dQ^2(d^2\sigma/dTd\cos\theta)$ calculated with $F_A = 0$ and σ^A is the cross section $d\sigma/dQ^2(d^2\sigma/dTd\cos\theta)$ calculated with $F_V = F_M = 0, F_A = 1$. The vector-axial cross section σ^{VA} , arising from the interference between the vector and axial currents can be written as

$$\sigma^{VA} = h[\sigma(F_A = 1) - \sigma^V - \sigma^A], \quad (13)$$

where $\sigma(F_A = 1)$ is the $d\sigma/dQ^2(d^2\sigma/dTd\cos\theta)$ cross section, calculated with $F_A(Q^2)=1$.

The flux integrated cross section can be written as a sum of the flux integrated QE and $2p - 2h$ MEC contributions

$$\left\langle \frac{d\sigma}{dQ^2}(Q^2) \right\rangle = \left\langle \frac{d\sigma_{QE}}{dQ^2}(Q^2) \right\rangle + \left\langle \frac{d\sigma_{MEC}}{dQ^2}(Q^2) \right\rangle, \quad (14)$$

where

$$\left\langle \frac{d\sigma_j}{dQ^2}(Q^2) \right\rangle = \int D_\nu(\varepsilon_i) \frac{d\sigma_j}{dQ^2}(Q^2, \varepsilon_i) d\varepsilon_i, \quad (15)$$

and $j = QE, MEC$. The weight functions D_ν are defined as

$$D_\nu(\varepsilon_i) = I_\nu(\varepsilon_i)/\Phi_\nu, \quad (16)$$

where $I_\nu(\varepsilon_i)$ is the neutrino spectrum and Φ_ν is the integral neutrino flux.

The value of $F_A(Q^2)$ as a function of Q^2 can be extracted as the solution to the equation

$$\left\langle \frac{d\sigma_{QE}}{dQ^2}(Q^2) \right\rangle = \left\langle \frac{d\sigma}{dQ^2}(Q^2) \right\rangle - \left\langle \frac{d\sigma_{MEC}}{dQ^2}(Q^2) \right\rangle, \quad (17)$$

using the neutrino CCQE-like scattering data for $\langle d\sigma^\nu/dQ^2 \rangle$ and

$$\left\langle \frac{d\sigma_{QE}}{dQ^2}(Q^2) \right\rangle = \langle \sigma^V(Q^2) \rangle + F_A^2(Q^2) \langle \sigma^A(Q^2) \rangle + h F_A(Q^2) \langle \sigma^{VA}(Q^2) \rangle, \quad (18)$$

where $\langle \sigma^j(Q^2) \rangle$ are the flux-integrated vector, axial and vector-axial ($j = V, A, VA$) cross sections. Note, that the values of the axial form factor extracted from the CCQE-like cross sections are model dependent and implicitly include the uncertainties in the F_V , F_M , ν_μ -flux, and $2p - 2h$ MEC contributions.

III. RESULTS AND ANALYSIS

Our main interest is to show the capability of the present model, RDWIA+MEC, to describe successfully the MiniBooNE neutrino scattering data and calculate within this approach the CCQE-like flux-integrated cross sections at energies available at the NOvA experiment.

A. Fit of the RDWIA+MEC model to the neutrino MiniBooNE data

The MiniBooNE neutrino data set [9], obtained in a kinematic range that significantly overlaps with the range available to the NOvA experiment, is used in the CCQE-like fit. These data have been released as flux-integrated double-differential cross section $d^2\sigma/dT d\cos\theta$ and as differential cross section $d\sigma/dQ^2$ in the range $0 < Q^2 < 2$ (GeV/c)². The data release included the diagonal elements of the shape-only covariant matrix for each

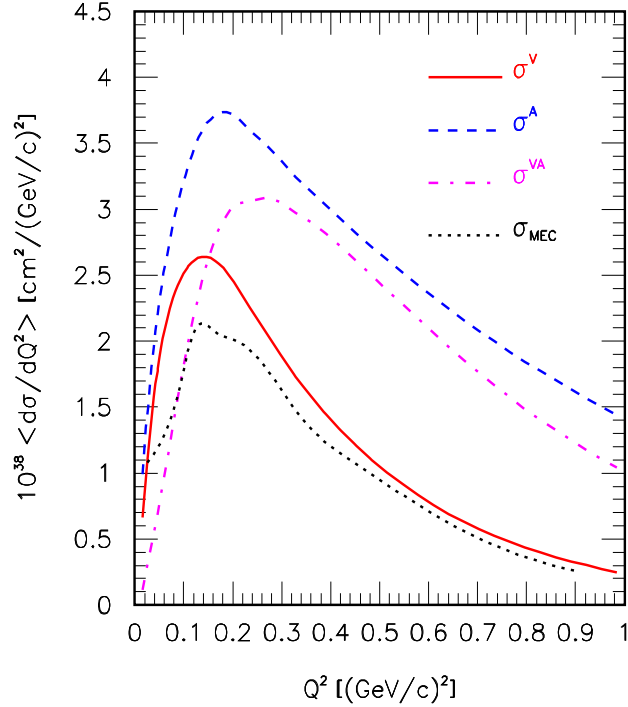


FIG. 1: Flux-integrated $\langle\sigma^V\rangle$ (solid line), $\langle\sigma^A\rangle$ (dashed line), $\langle\sigma^{VA}\rangle$ (dashed-dotted line), and $\langle d\sigma_{MEC}/dQ^2\rangle$ (dotted line) cross sections of ν_μ scattering on ^{12}C as functions of Q^2 .

bin and correlations between bins were not presented. The normalization uncertainty was given as 10.7%. In our analysis we use the CCQE corrected sample with purity 77%. In the MiniBooNE antineutrino data set [11] the correction algorithm for the antineutrino data is more complicated than for neutrino mode sample, due to the relatively high ν_μ contamination in the $\bar{\nu}_\mu$ beam. There is also a large $\text{CC}1\pi^-$ background in the $\bar{\nu}_\mu$ CCQE sample, as most of the π^- are absorbed. As a result of the two large backgrounds in the antineutrino sample, the purity of the antineutrino CCQE-like sample is 61%.

To extract the values of the axial form factor $F_A(Q^2)$ as a function of Q^2 , using the measured neutrino flux-integrated $\langle d\sigma/dQ^2\rangle$ cross section, we calculated the $\langle\sigma^V\rangle$, $\langle\sigma^A\rangle$, $\langle\sigma^{VA}\rangle$, and $\langle d\sigma_{MEC}/dQ^2\rangle$ cross sections with the booster neutrino beam line ν_μ flux [9]. In Fig. 1 these cross sections for ν_μ scattering on ^{12}C are shown against Q^2 . In Fig. 2(a) we show the measured flux-integrated $\langle d\sigma/dQ^2\rangle$ as a function of Q^2 . To extract the values of F_A this cross section with the shape-only error was used in Eq. (17). The results, $F_A(Q^2)$ as a function of Q^2 , are shown in Fig. 2(b). Also shown in this figure are the results from Ref. [47],

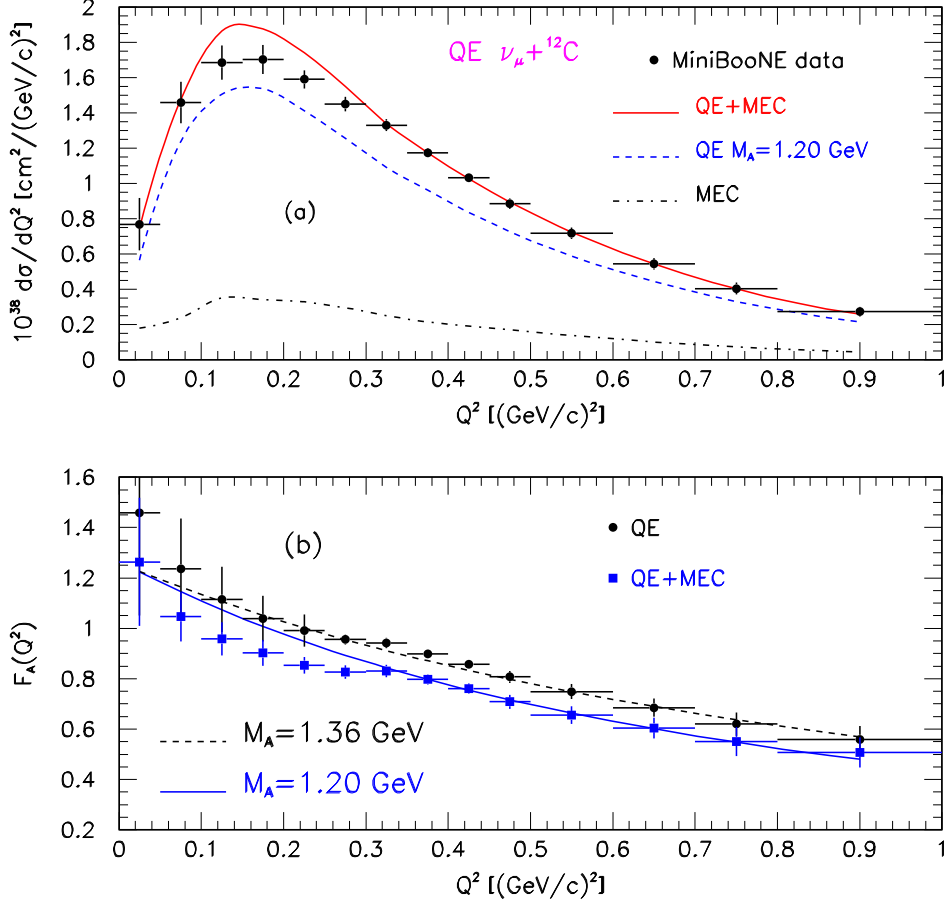


FIG. 2: Flux-integrated $d\sigma/dQ^2$ cross section per target neutron for the ν_μ CCQE-like scattering (upper panel) and axial form factor $F_A(Q^2)$ extracted from the MiniBooNE data as functions of Q^2 . Upper panel: Calculations from the RDWIA+MEC (solid line), RDWIA (dashed line) with $M_A = 1.2$ GeV, and $2p - 2h$ MEC contributions (dashed-dotted line). Lower panel: Filled squares (filled circles) are the axial form factor extracted within the RDWIA+MEC (RDWIA), and the solid (dashed) line is the result of the dipole parametrization with $M_A = 1.2(1.36)$ GeV.

obtained within the RDWIA, *i.e.* without the $2p - 2h$ MEC contributions. The axial form factor values extracted in the RDWIA approach agree well with the dipole parametrization with $M_A = 1.36$ GeV. As observed, results in Fig. 2(b) clearly show the relevant role played by the $2p - 2h$ MEC contributions. The values of F_A obtained with the RDWIA are

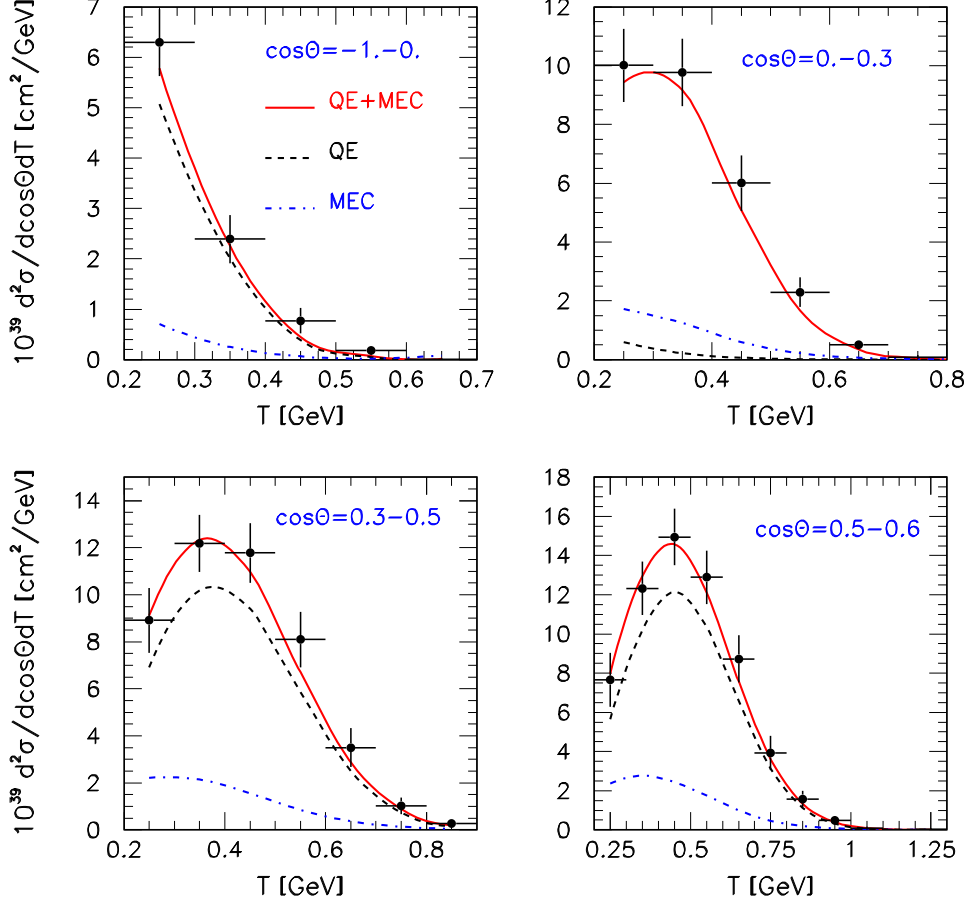


FIG. 3: Flux-integrated $d^2\sigma/dTd\cos\theta$ cross section per target neutron for the ν_μ CCQE-like scattering as a function of muon kinetic energy for the four muon scattering angle bins: $\cos\theta = (-1-0)$, $(0-0.3)$, $(0.3-0.5)$, and $(0.5-0.6)$. As shown in the key, cross sections were calculated within the RDWIA+MEC approach. The QE and $2p-2h$ MEC contributions are also presented separately. The MiniBooNE data are shown as points with the shape error only.

higher and decrease with Q^2 more slowly than corresponding values extracted within the RDWIA+MEC approach.

We also performed a shape-only fit the RDWIA+MEC model to the MiniBooNE neutrino data with only the axial mass M_A as a variable model parameter. Ref. [60] shows that the best fit parameter values are not significantly altered by including the MiniBooNE normal-

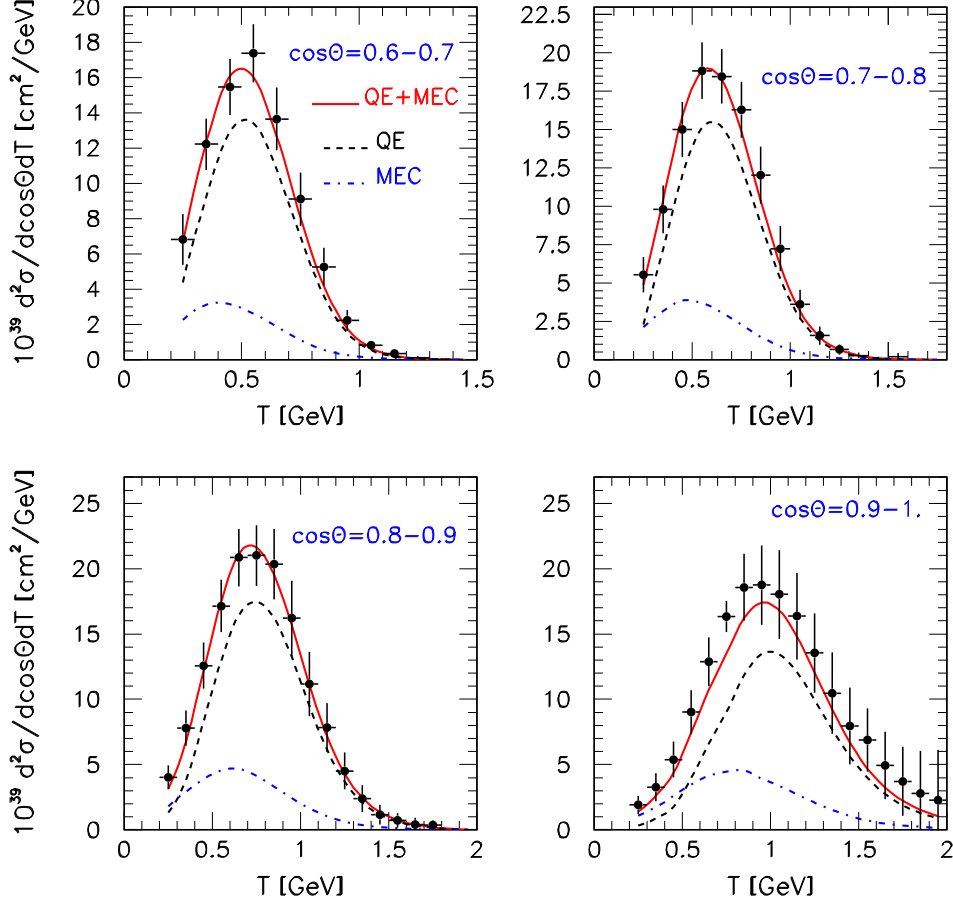


FIG. 4: Same as Fig. 3 but for muon scattering angle bins: $\cos\theta = (0.6-0.7)$, $(0.7-0.8)$, $(0.8-0.9)$, and $(0.9-1)$.

ization uncertainties in the CCQE fit. The fits were made to the single-differential $d\sigma/dQ^2$ (1D fit), double-differential $d^2\sigma/dT d\cos\theta$ (2D fit) cross sections, and their combination (1D+2D main fit), using the χ^2 statistic

$$\chi^2 = \sum_{k=1}^N \left[\frac{(d\sigma/dQ^2)_k^{data} - (d\sigma/dQ^2)_k^{th}}{\Delta(d\sigma/dQ^2)_k} \right]^2 \rightarrow 1D$$

$$+ \sum_{l=1}^M \left[\frac{(d^2\sigma/dT d\cos\theta)_l^{data} - (d^2\sigma/dT d\cos\theta)_l^{th}}{\Delta(d^2\sigma/dT d\cos\theta)_l} \right]^2 \rightarrow 2D, \quad (19)$$

where $\Delta(d\sigma/dQ^2)_k$ and $\Delta(d^2\sigma/dT d\cos\theta)_l$ are the diagonals of the MiniBooNE shape-only

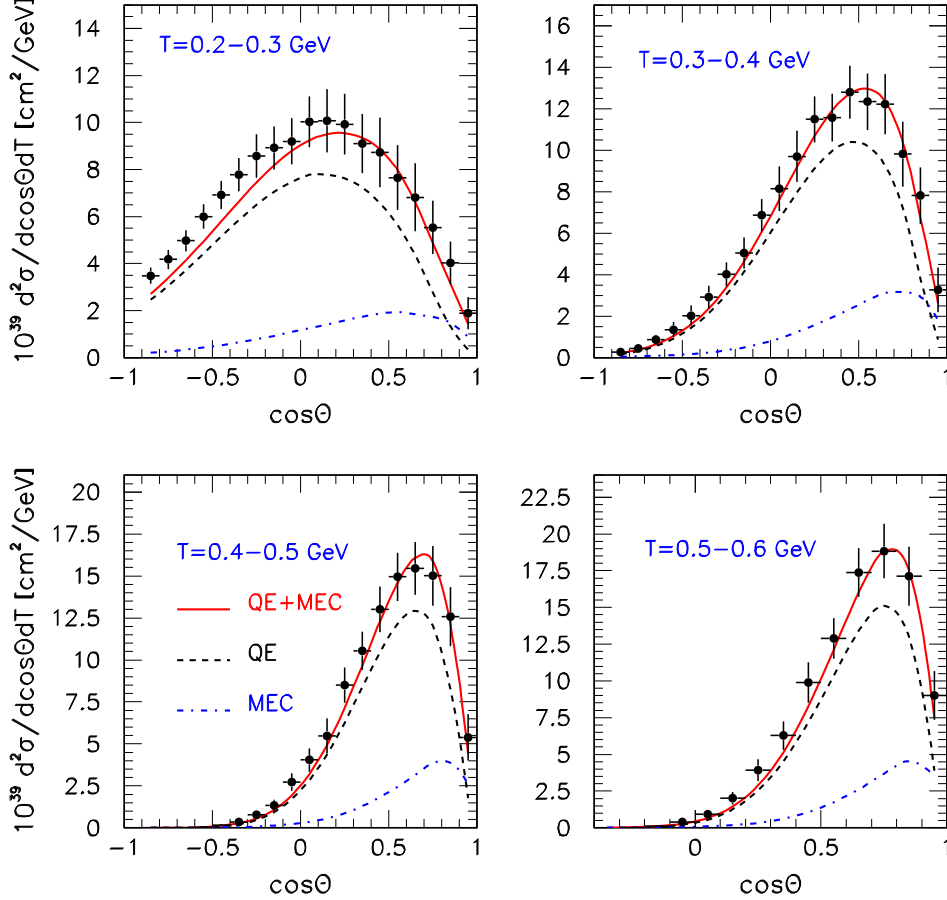


FIG. 5: Flux-integrated $d^2\sigma/dT d\cos\theta$ cross section per target neutron for the ν_μ CCQE-like scattering as a function of $\cos\theta$ for the four muon kinetic energy bins: $T(\text{GeV})=(0.2-0.3)$, $(0.3-0.4)$, $(0.4-0.5)$, and $(0.5-0.6)$. As shown in the key, cross sections were calculated within the RDWIA+MEC approach. The QE and $2p-2h$ MEC contributions are also presented. The MiniBooNE data are shown as points with the shape error only.

covariance matrices for neutrino results. The following best fit χ^2 and M_A values are obtained: $\chi^2/\text{DOF}=19/13$ and $M_A = 1.17 \pm 0.03$ GeV for the 1D fit, $\chi^2/\text{DOF}=62/136$ and $M_A = 1.24 \pm 0.09$ GeV for the 2D fit, and $\chi^2/\text{DOF}=111/150$ and $M_A = 1.20 \pm 0.06$ GeV for the 1D+2D main fit. Although there is a difference between the best fit M_A values, the errors from the fits cover this difference. Additionally, the value of $M_A = 1.20 \pm 0.06$ GeV from

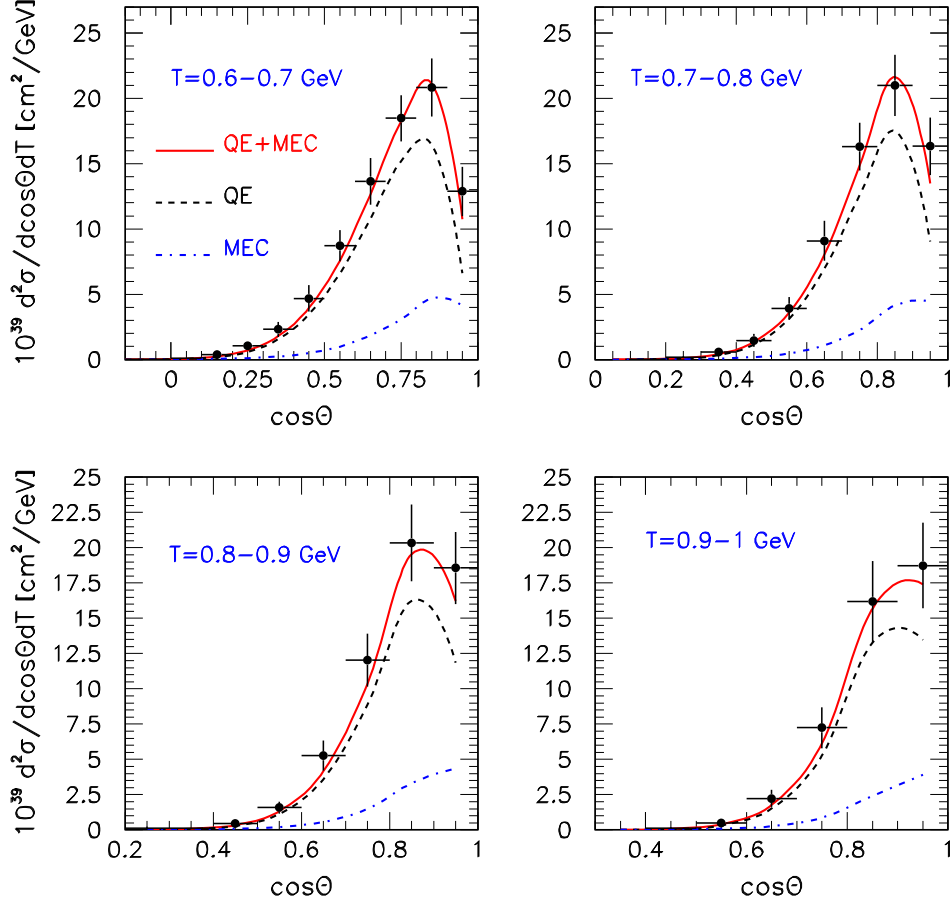


FIG. 6: Same as Fig. 5 but for the four muon kinetic energy bins: $T(\text{GeV})=(0.6-0.7)$, $(0.7-0.8)$, $(0.8-0.9)$, and $(0.9-1)$.

main fit is in agreement within the errors with the best fit value of $M_A = 1.15 \pm 0.03$ GeV obtained from the main CCQE fit of the MiniBooNE and MINERvA data in Refs. [46, 60]. The best fit $d\sigma/dQ^2$ distribution is compared with the data in Fig. 2(a). The result of the dipole parametrization of $F_A(Q^2)$ with $M_A = 1.2$ GeV is shown in Fig. 2(b). There is an overall agreement between the RDWIA+MEC $d\sigma/dQ^2$ cross section and the data, but the model slightly overestimate the data in the range $0.08 < Q^2 < 0.3$ (GeV/c) 2 . In Figs. 3, 4, 5, 6, and 7 we show double differential cross sections calculated with $M_A = 1.2$ GeV. The results for $d^2\sigma/dT d\cos\theta$ cross sections against the kinematic energy of the muon are shown

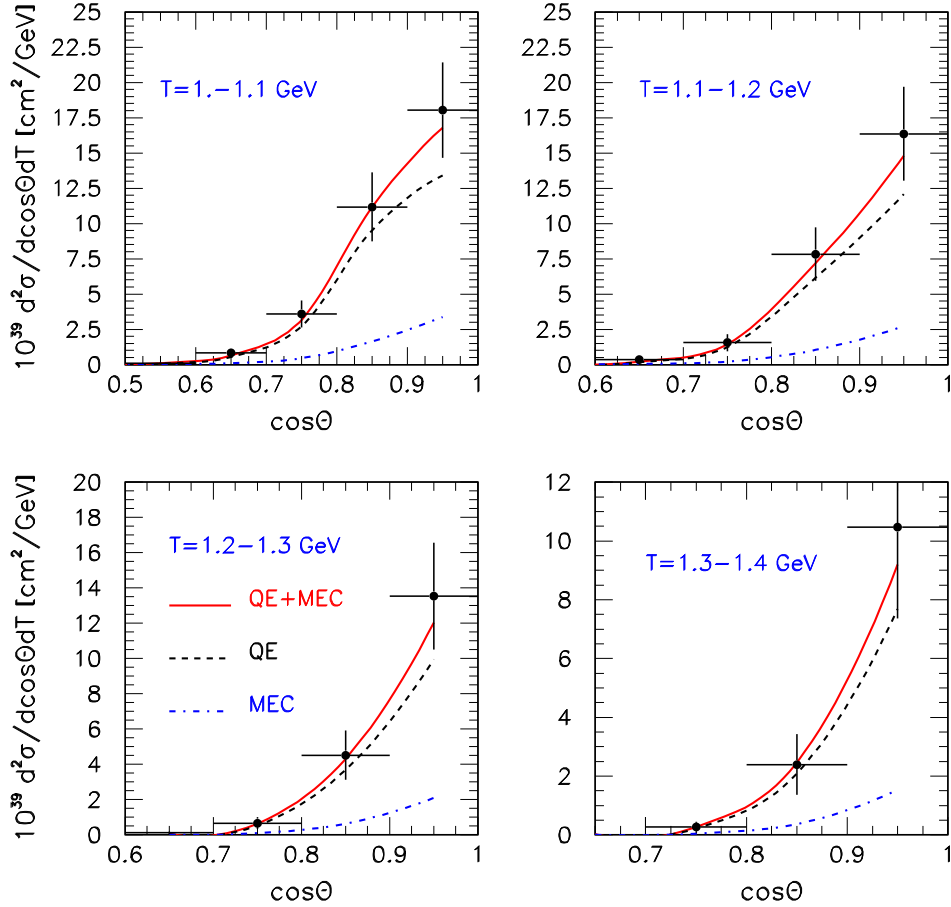


FIG. 7: Same as Fig. 5 but for the four muon kinetic energy bins: $T(\text{GeV})=(1.-1.1)$, $(1.1-1.2)$, $(1.2-1.3)$, and $(1.3-1.4)$.

in Figs. 3, 4. We present a large variety of kinematical situations where each panel refers to results averaged over a particular muon angular bin. As observed, the model tends to slightly underestimate the data for most forward angles, i.e. $0.9 < \cos\theta < 1$. As the scattering angle increases, the RDWIA+MEC prediction agrees well with the data. Results in Figs. 3 and 4 clearly show that the $2p-2h$ MEC contributions are essential in order to describe data. The contribution of these effects are comparable with the genuine QE process, being of order 25% and increasing up to 30% at low Q^2 . In Figs. 5, 6, and 7 we present the results averaged over the muon kinetic energy bins as functions of the muon scattering angle. These graphs

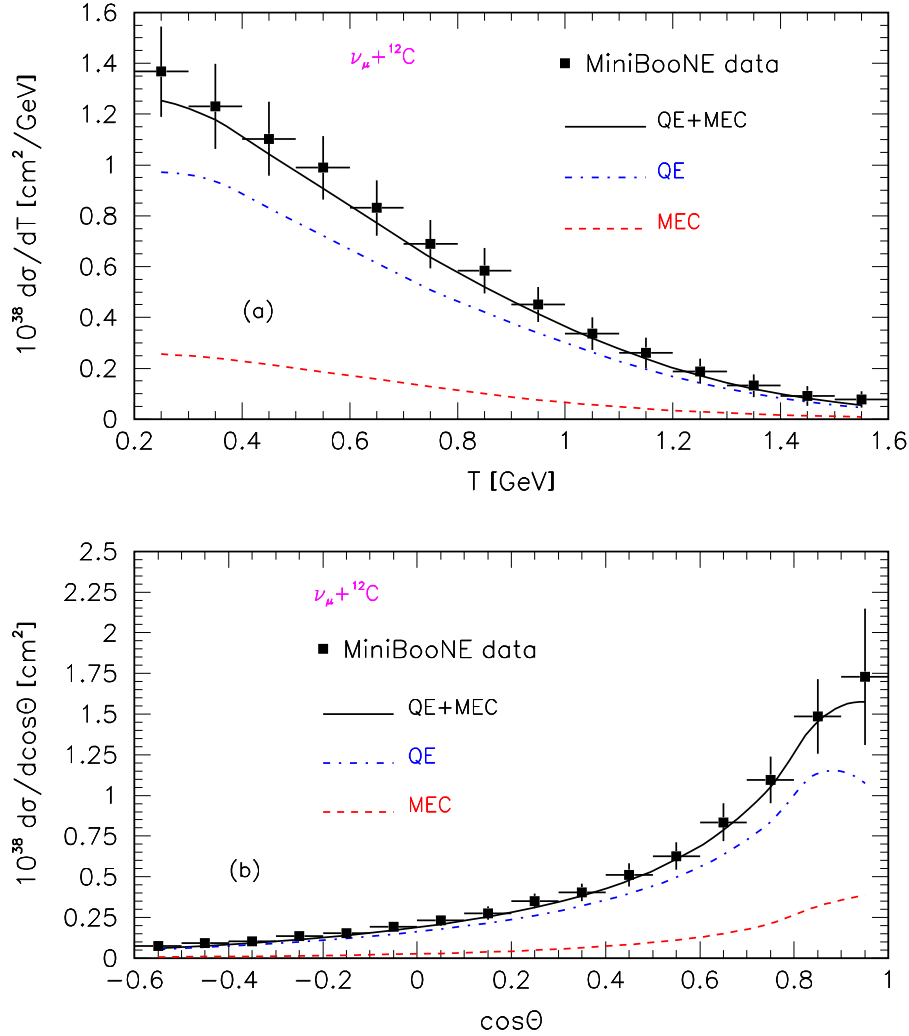


FIG. 8: Flux-integrated $d\sigma/dT$ cross section as a function of muon kinetic energy (upper panel) and $d\sigma/d\cos\theta$ cross section for $T > 0.2$ GeV as a function of muon scattering angle (lower panel) for the ν_μ CCQE-like scattering per target neutron. As shown in the key, cross sections were calculated within the RDWIA+MEC. The RDWIA and $2p - 2h$ MEC results are also presented separately. The MiniBooNE data are shown as points with the shape error only.

complement the previous ones, and show that the RDWIA+MEC model is able to reproduce the data. There is a good agreement between the calculated results and the data within experimental error. In the region $0.2 < T < 0.3$ GeV and $-1 < \cos\theta < -0.2$ the model result is slightly lower than the measured cross section, and the difference decreases with muon energy. In Fig. 8 results are presented for the MiniBooNE flux-integrated CCQE-like

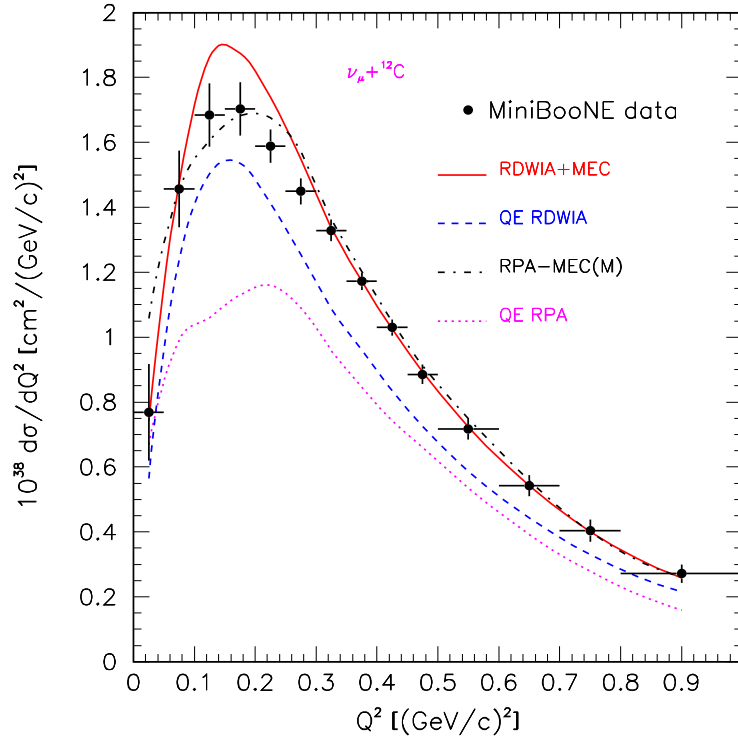


FIG. 9: Flux-integrated $d\sigma/dQ^2$ cross section per target neutron for the ν_μ CCQE-like and CCQE processes as a function of Q^2 . As shown in the key, cross sections were calculated within the RDWIA+MEC ($M_A = 1.2$ GeV) and RPA-MEC [34] models. The CCQE contributions calculated in the RDWIA and RPA approaches are also presented separately. The MiniBooNE data are shown as points with the shape-only error.

$d\sigma/dT$ differential cross section as a function of the muon kinetic energy (upper panel) and $d\sigma/d\cos\theta$ cross section versus of muon scattering angle (lower panel). The measured $d\sigma/dT$ ($d\sigma/d\cos\theta$) cross section with the shape-only error was obtained by summing the double-differential cross section over $\cos\theta$ bins (T bins) presented in Tables VI and VII in Ref. [9]. The integration over muon kinetic energy has been performed in the range $0.2 < T < 2$ GeV. As shown, the RDWIA+MEC model with $M = 1.2$ GeV is capable of reproducing the magnitude as well as the shape of the experimental cross sections.

In Figs. 9, 10, and 11 the MiniBooNE neutrino flux-averaged CCQE-like differential cross sections calculated within the different approached are presented. In Fig. 9 we show the $d\sigma/dQ^2$ cross sections as measured in Ref. [9] and as calculated in the RDWIA+MEC and RPA-MEC [34] models. Also shown are CCQE cross sections obtained in these approaches.

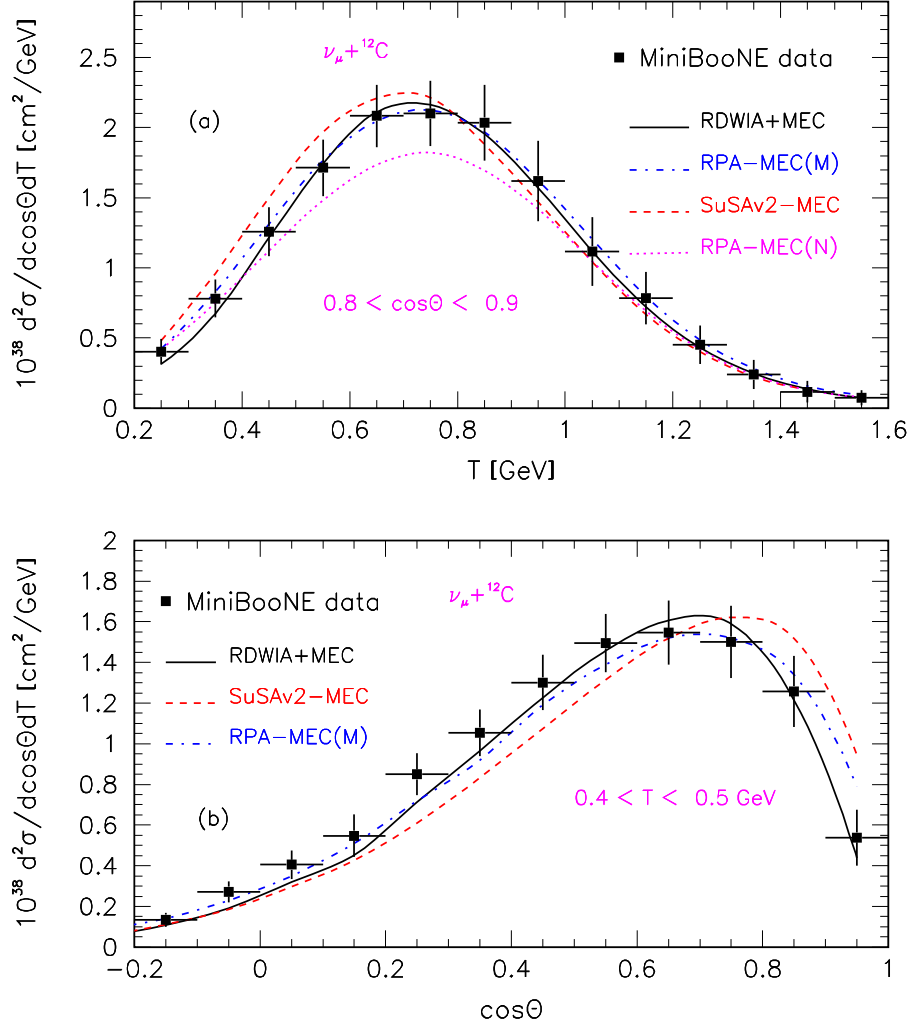


FIG. 10: Flux-integrated $d^2\sigma/dTdcos\theta$ cross section per target neutron for the CCQE-like scattering. Upper panel: Cross sections calculated within the RDWIA+MEC (solid line), RPA-MEC (dashed-dotted line) [34], SuSAv2-MEC (dashed line), and RPA-MEC (dotted line) [36] models for $0.8 < \cos\theta < 0.9$ as functions of muon kinetic energy. Lower panel: Cross sections calculated in the RDWIA+MEC (solid line), SuSAv2-MEC (dashed line), and RPA-MEC (dashed-dotted line) [34] approaches for $0.4 < T < 0.5$ GeV as functions of muon scattering angle. The MiniBooNE data are shown as points with the shape-only error.

From the figure one can observe that these calculations describe well the experimental data at $Q^2 > 0.3$ (GeV/c)². The RDWIA+MEC model slightly overestimate the data in the range $0.08 < Q^2 < 0.3$ (GeV/c)² and in the case of the RPA+MEC approach a tendency

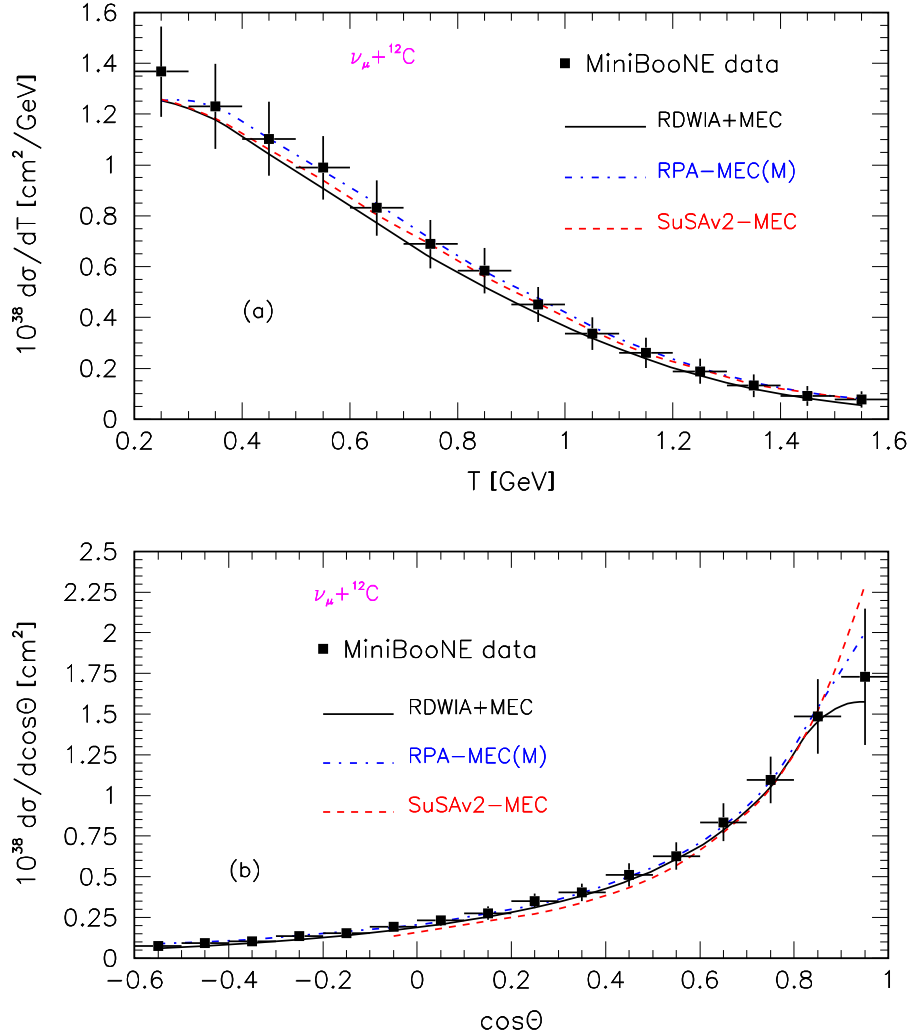


FIG. 11: Flux-integrated $d\sigma/dT$ cross section as a function of muon kinetic energy (upper panel) and $d\sigma/d\cos\theta$ cross section for $T > 0.2$ GeV as a function of muon scattering angle (lower panel) for the CCQE-like scattering per target neutron. As shown in the key, cross sections were calculated within the RDWIA+MEC, SuSAv2-MEC, and RPA-MEC [34] models. The MiniBooNE data are shown as points with the shape-only error.

to overestimate the data appears at low $Q^2 < 0.06$ (GeV/c) 2 . In the range of $Q^2 < 0.3$ (GeV/c) 2 , which is affected by RPA quenching, the CCQE cross sections calculated in the RDWIA with $M_A = 1.2$ GeV is $\approx 30\%$ larger than those obtained in Ref. [34] and the discrepancy decreases with Q^2 up to 12% at $Q^2 \approx 0.9$ (GeV/c) 2 . In Fig. 10 we show the double-differential $d^2\sigma/dT d\cos\theta$ cross sections calculated in the RDWIA+MEC, SuSAv2-

MEC [59], and RPA-MEC [34, 36] approaches. For the sake of illustration in Fig. 10(a) the results are given for $0.8 < \cos \theta < 0.9$ as functions of the muon kinetic energy. As one can observe, the results of the RDWIA+MEC, SuSAv2-MEC, and RPA-MEC [34] models are in agreement with data. In the case of the RPA-MEC result [36] a tendency to underestimate the MiniBooNE data appears. In Fig. 10(b) the results are given for muon kinetic energy bin $0.4 < T < 0.5$ GeV as functions of the muon scattering angle. As shown, the results obtained within the RDWIA+MEC and RPA-MEC [34] models agree well with data. On the other hand, a difference between the SuSAv2-MEC result and data is observed. The flux-averaged differential cross sections $d\sigma/dT$ and $d\sigma/d\cos\theta$ (for $T > 0.2$ GeV), calculated in the RDWIA+MEC, SuSAv2-MEC, and RPA-MEC [34] approaches are presented in Fig. 11, which shows $d\sigma/dT$ as a function of muon kinetic energy and $d\sigma/d\cos\theta$ as a function of the muon scattering angle. Also shown are the MiniBooNE measured cross sections with the shape-only error. There is a good agreement within the errors between the calculated results and data.

B. Calculation of neutrino CCQE-like differential cross sections at energies of the NOvA experiment

Within the RDWIA+MEC approach with $M_A = 1.2$ GeV, which was successfully tested against the MiniBooNE neutrino data, we estimated the neutrino CCQE-like flux-integrated differential cross sections at energies available at the NOvA experiment [49, 50]. The NOvA detectors are situated 14 mrad off the neutrino main injector (NuMI) beam axis, so they expose a relatively narrow band $\sim 0.5 - 5$ GeV of neutrino energies, centered at 2 GeV [61]. This flux is used in the calculation of the NOvA flux-integrated differential cross sections.

In the fiducial region of the NOvA near detector (ND) the liquid scintillator (CH_2) comprises 63% of the detector mass. Mass weight for this detector component is as follows: ^{12}C - 66.8%, ^{35}Cl - 16.4%, ^1H - 10.5%, ^{48}Ti - 3.3%, ^{16}O - 2.6%, and others - 0.4% [62]. So, the ND is dominated by carbon, chlorine, and hydrogen. We assumed that the NOvA CCQE-like scattering sample consists of two processes: scattering on ^{12}C and ^{35}Cl . The mass weight of carbon α_c and chlorine α_{Cl} was re-scaled for neutrino scattering as $\alpha_C = 0.806$, $\alpha_{Cl} = 0.194$, and $\alpha_c + \alpha_{Cl} = 1$. In Ref. [47] we calculated within the RDWIA the CCQE differential cross sections for (anti)neutrino scattering on ^{40}Ar . The difference between the

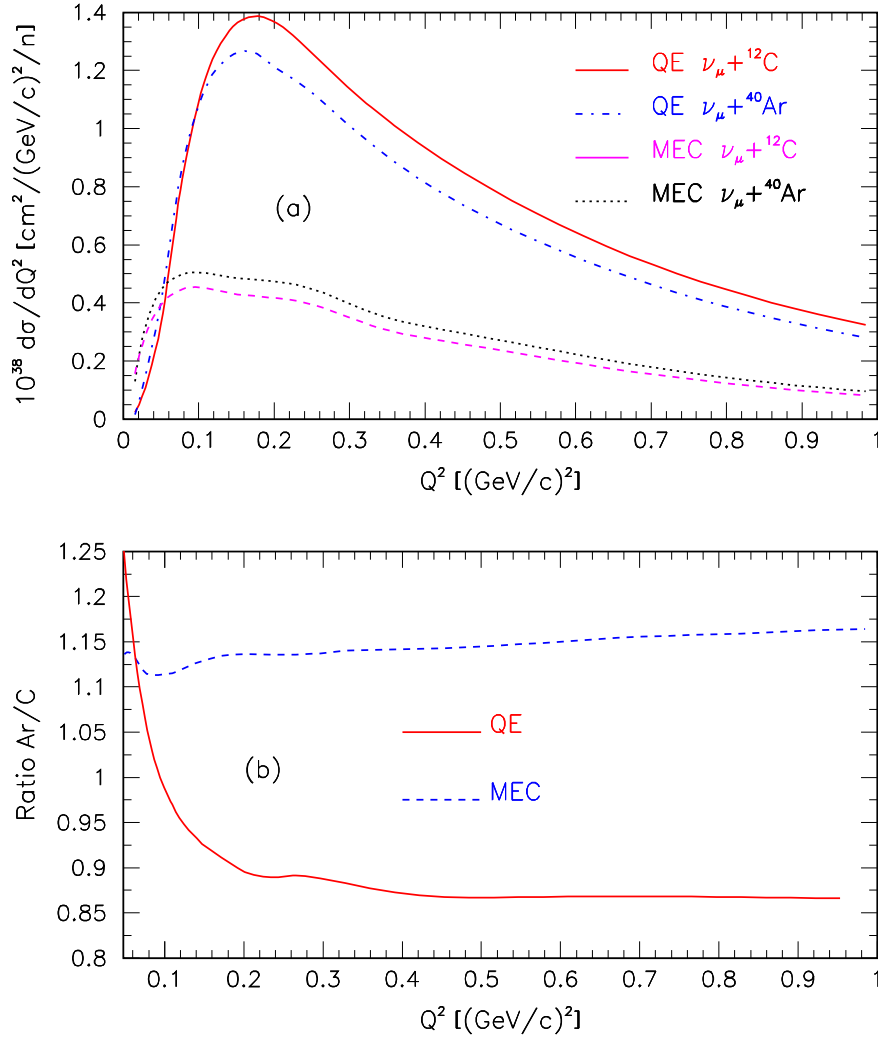


FIG. 12: NOvA flux-integrated $d\sigma/dQ^2$ cross sections per target neutron for the ν_μ CCQE and $2p-2h$ MEC scattering (upper panel) and ratio R_{QE} and R_{MEC} (lower panel) as functions of Q^2 . As shown in the key, cross sections were calculated for neutrino scattering on ${}^{12}\text{C}$ and ${}^{40}\text{Ar}$.

nuclear structures of ${}^{40}\text{Ar}$ and ${}^{35}\text{Cl}$ is not significant. Therefore the NOvA CCQE-like differential cross sections were estimated for neutrino scattering on carbon and argon, here-with the $2p-2p$ MEC contributions for ${}^{40}\text{Ar}$ was calculated using the parameterizations for ${}^{12}\text{C}$ re-scaled for argon according to [63]. Then the NOvA neutrino scattering cross section per target neutron, *i.e.* the cross sections averaged over the ND mass weight, can be expressed as $\sigma_{MIX} = \alpha_C \sigma_C + \alpha_{Cl} \sigma_{Ar}$, where σ_c (σ_{Ar}) is the cross section of neutrino scattering on ${}^{12}\text{C}$ (${}^{40}\text{Ar}$).

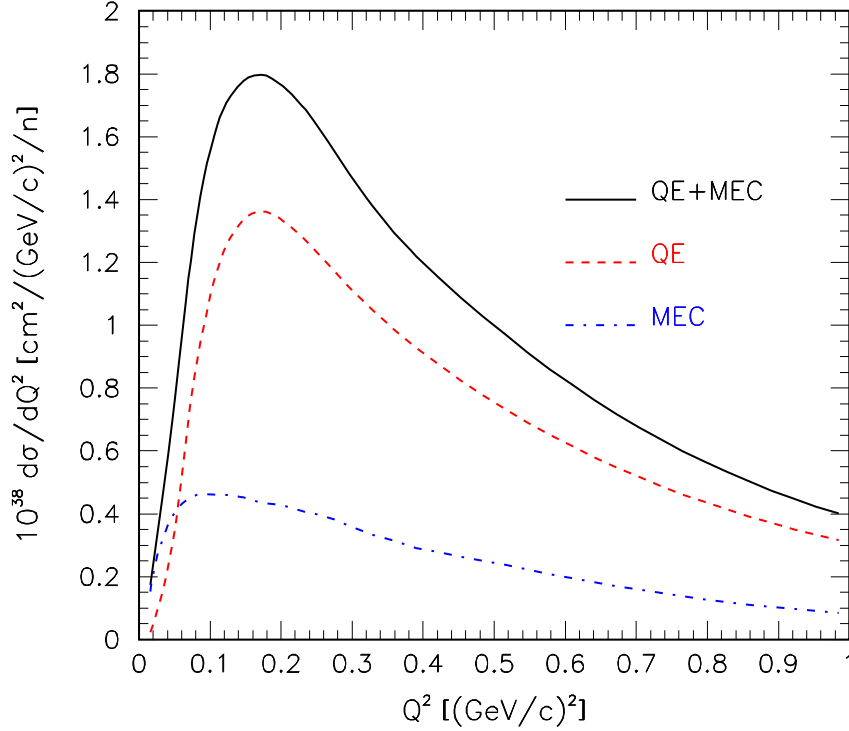


FIG. 13: NOvA flux-integrated $d\sigma/dQ^2$ cross sections per target neutron for the ν_μ CCQE-like scattering (solid line). The CCQE (dashed line) and $2p - 2h$ MEC (dashed-dotted line) results are also presented separately. The cross sections are shown as functions of Q^2 .

Fig. 12 contains the RDWIA+MEC model predictions corresponding to the NOvA flux-integrated $d\sigma/dQ^2$ cross sections per target neutron for neutrino scattering on ^{12}C and ^{40}Ar . The cross sections were calculated for the CCQE and $2p - 2h$ MEC processes in the region $T > 0.3$ GeV and $0.3 < \cos\theta < 1$. Also shown are the ratios $R_{QE} = (d\sigma/dQ^2)_{QE}^{Ar}/(d\sigma/dQ^2)_{QE}^C$ and $R_{MEC} = (d\sigma/dQ^2)_{MEC}^{Ar}/(d\sigma/dQ^2)_{MEC}^C$, where $(d\sigma/dQ^2)_{QE}^{Ar}[(d\sigma/dQ^2)_{QE}^C]$ and $(d\sigma/dQ^2)_{MEC}^{Ar}[(d\sigma/dQ^2)_{MEC}^C]$ are the CCQE and $2p-2h$ MEC cross sections per target neutron for neutrino scattering on ^{40}Ar (^{12}C), respectively. The figure clearly shows that the ratio R_{QE} reduces with Q^2 from 1.2 at $Q^2 \approx 0.04$ $(\text{GeV}/c)^2$ up to 0.87 at $Q^2 \approx 1$ $(\text{GeV}/c)^2$. On the other hand the ratio R_{MEC} increases slowly with Q^2 from 1.1 at $Q^2 \approx 0.1$ $(\text{GeV}/c)^2$ up to 1.17 at $Q^2 \approx 1$ $(\text{GeV}/c)^2$. Thus, the RDWIA+MEC model predicts that the CCQE differential cross section per target neutron reduces and $2p - 2h$ MEC contribution increases with the mass number of the target.

The results in Fig. 13 correspond to the flux-integrated NOvA $(d\sigma/dQ^2)_{MIX}$ cross section

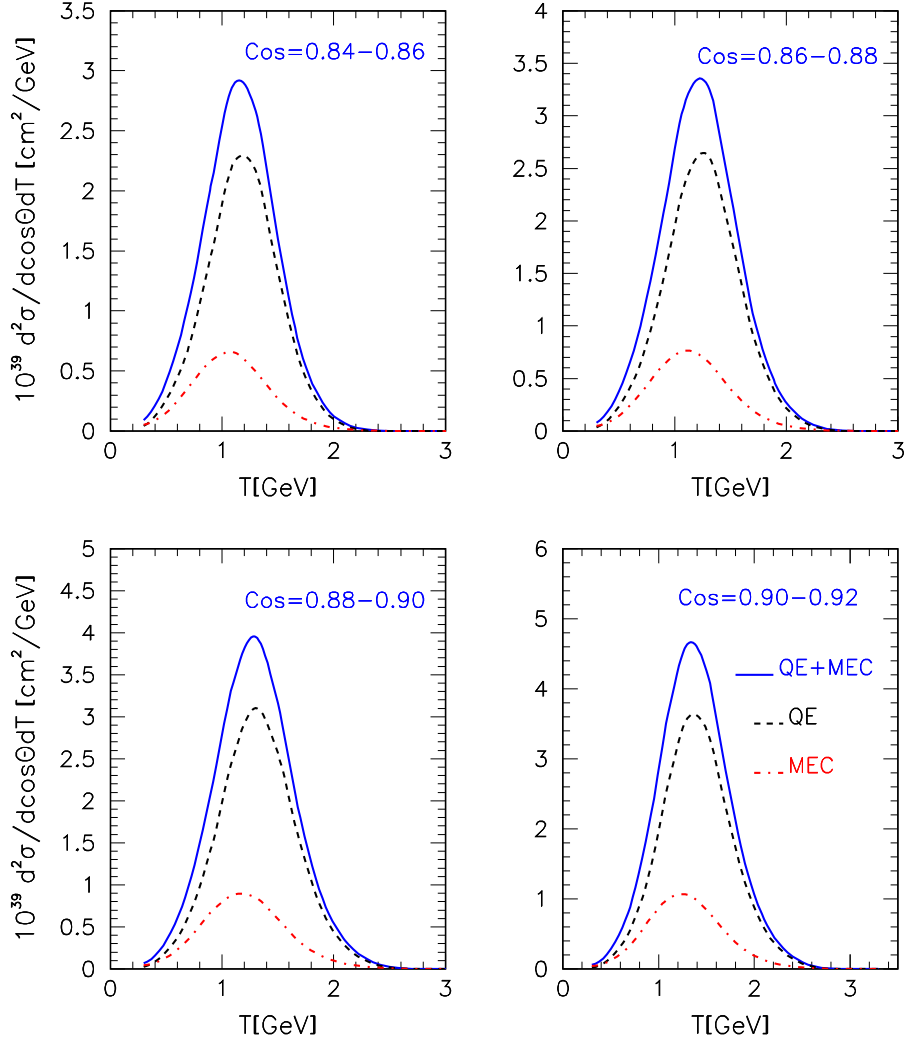


FIG. 14: NOvA flux-integrated $d^2\sigma/d\cos\theta dT$ cross section per target neutron for the ν_μ CCQE-like scattering as a function of muon kinetic energy for the four muon scattering angle bins: $\cos\theta=(0.84-0.86)$, $(0.86-0.88)$, $(0.88-0.90)$, and $(0.90-0.92)$. As shown in the key, cross section was calculated within the RDWIA+MEC. The CCQE and $2p-2h$ MEC contributions are also shown separately.

per target neutron of the CCQE-like neutrino scattering. Also shown are the contributions of the CCQE and $2p-2h$ MEC processes. The ratio $R = (d\sigma/dQ^2)_{MIX}/(d\sigma/dQ^2)_C$ is about 0.98 in the range $0.1 < Q^2 < 1$ (GeV/c)², *i.e.* the NOvA CCQE-like cross section per target nucleon for neutrino scattering in the NOvA ND is, practically, the same as one for scattering on carbon.

In Figs. 14 and 15 we present the flux-integrated CCQE-like double differential cross

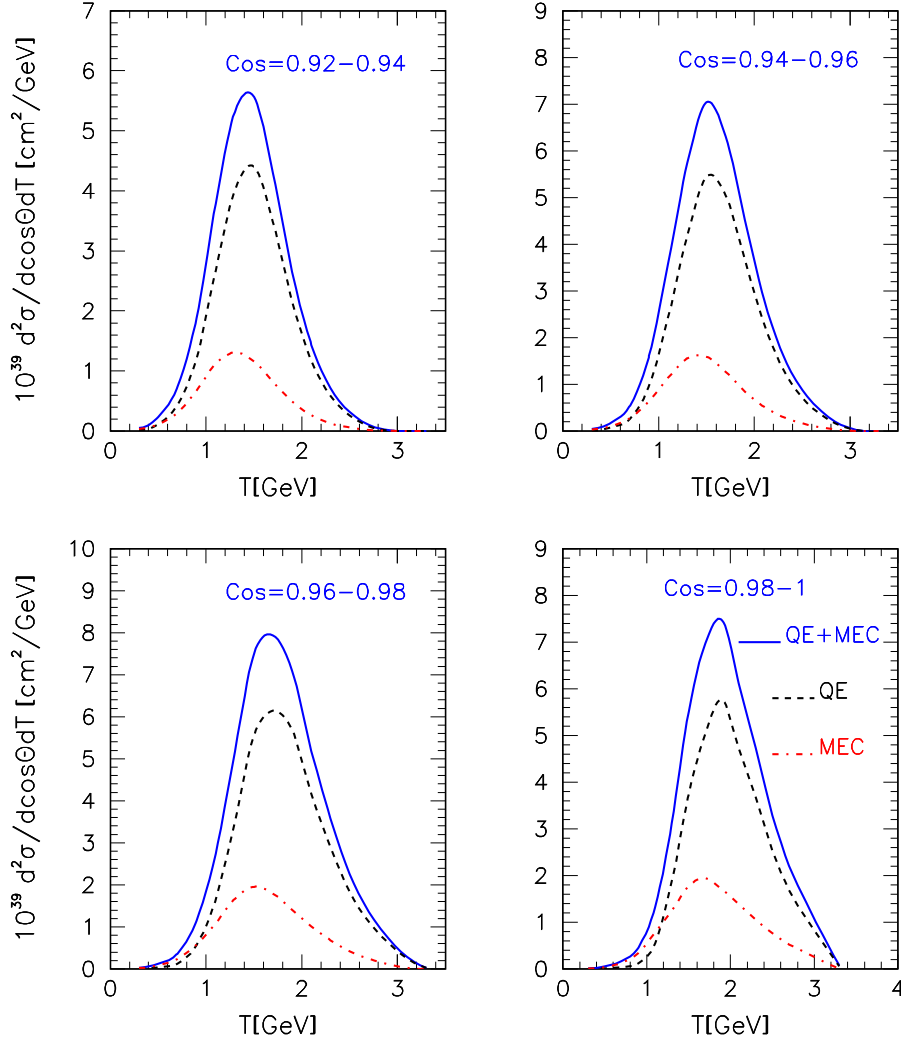


FIG. 15: Same as Fig. 14 but for muon scattering angle bins: $\cos\theta=(0.92-0.94)$, $(0.94-0.96)$, $(0.96-0.98)$, and $(0.98-1)$.

sections per neutron predicted for the NOvA experiment. The graphs are plotted against the muon kinetic energy and each panel corresponds to a bin in the muon scattering angle. The double differential cross sections averaged over muon kinetic energy bins are shown in Figs. 16 and 17. In these figures we show the separate contributions of the genuine QE and $2p-2h$ MEC processes. The NOvA flux-integrated CCQE-like ν_μ cross sections per target neutron $d\sigma/dT$ as a function of the muon kinetic energy and $d\sigma/d\cos\theta$ versus muon scattering angle are presented in Fig. 18. The pure QE and $2p-2h$ MEC results are also shown separately. Integration of the double differential cross section over muon scattering

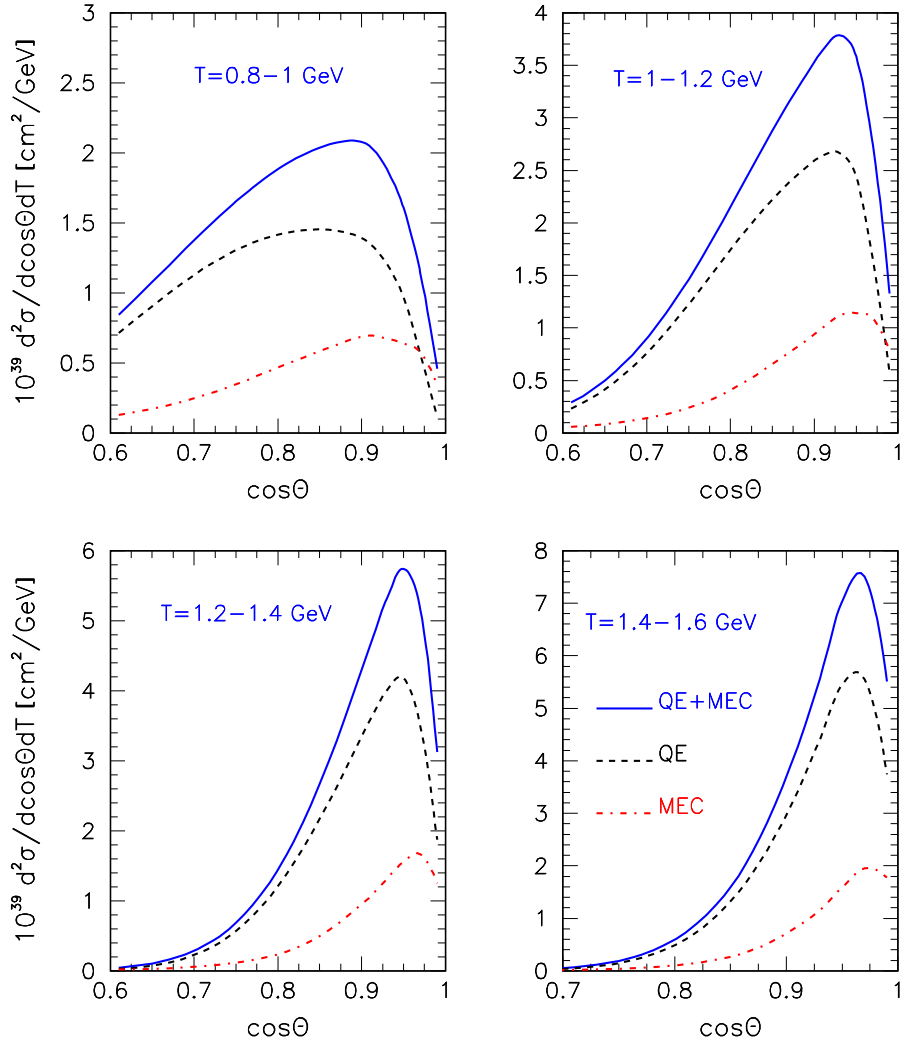


FIG. 16: NOvA flux-integrated $d^2\sigma/d\cos\theta dT$ cross section per target neutron for the ν_μ CCQE-like scattering as a function of muon kinetic energy for the four muon kinetic energy bins: $T(\text{GeV})=(0.8-1)$, $(1-1.2)$, $(1.2-1.4)$, and $(1.4-1.6)$. As shown in key, cross section was calculated within the RDWIA+MEC. The CCQE and $2p-2h$ MEC contributions are also presented separately.

angle has been performed in the range $0.6 < \cos\theta < 1$, for calculation of the $d\sigma/dT$ cross section and over muon kinetic energy in the range $0.2 < T < 3.5$ GeV, for evaluation of the $d\sigma/d\cos\theta$ cross section.

The ratio of the neutrino flux-integrated differential CCQE-like $(d\sigma/dQ^2)_{QE+MEC}$ cross section to the genuine QE $(d\sigma/dQ^2)_{QE}$ one, $R_{MEC} = (d\sigma/dQ^2)_{QE+MEC}/(d\sigma/dQ^2)_{QE}$, calculated for the MiniBooNE and NOvA experiments are shown in Fig. 19. As observed, in the

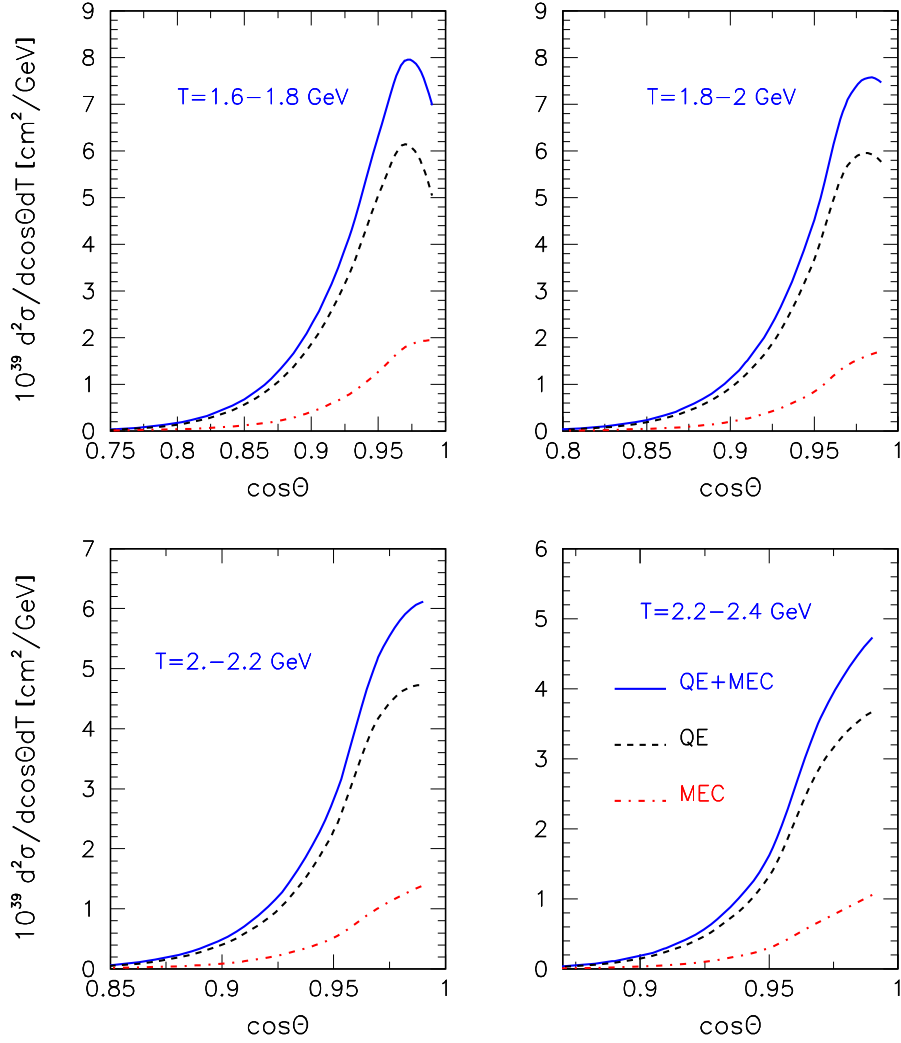


FIG. 17: Same as Fig. 16 but for muon kinetic energy bins: $T(\text{GeV})=(1.6-1.8)$, $(1.8-2.0)$, $(2.0-2.2)$, and $(2.2-2.4)$.

NOvA case the contribution of the $2p-2h$ MEC is about 8% higher than in the MiniBooNE experiment. This can be connected with the NOvA neutrino flux that is centered at neutrino energy ≈ 2 GeV, whereas the MiniBooNE neutrino flux has maximum at the energy ≈ 0.7 GeV. As was discussed earlier, the Δ -peak is the main contribution to the pion production cross section which increases with neutrino energy in the range up to 3 GeV.

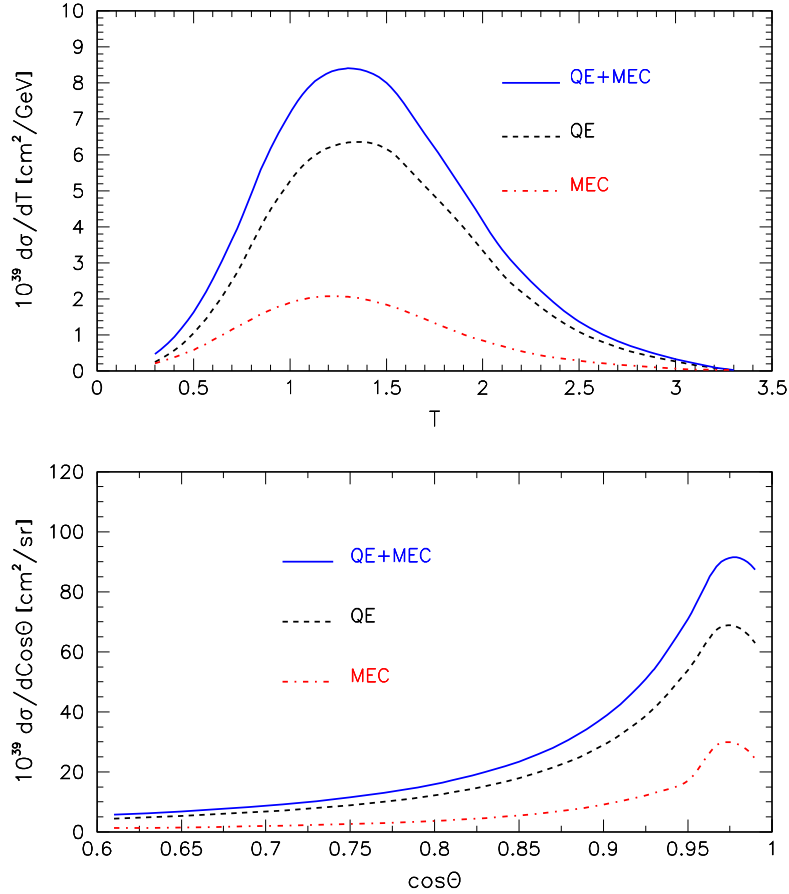


FIG. 18: NOvA flux-integrated $d\sigma/dT$ cross sections for $0.6 < \cos\theta < 1$ as a function of muon kinetic energy (upper panel) and $d\sigma/d\cos\theta$ cross section for $0.2 < T < 3.5$ GeV as a function of muon scattering angle (lower panel) for the ν_μ CCQE-like scattering per target neutron. As shown in the key, cross sections were calculated within the RDWIA+MEC approach. The CCQE and $2p - 2h$ MEC contributions are also shown.

IV. CONCLUSIONS

In this article we analyzed the MiniBooNE neutrino data within the RDWIA+MEC model. This model has been validated in the vector sector by describing the set of inclusive electron scattering ^{12}C data. We performed a shape-only fit of the RDWIA+MEC approach to the data with only the nucleon axial mass, as variable model parameter. A best fit value of $M_A = 1.2 \pm 0.06$ GeV was obtained. This value is in agreement within the errors with the best fit value of $M_A = 1.15 \pm 0.03$ GeV obtained from the CCQE main fit of the MiniBooNE

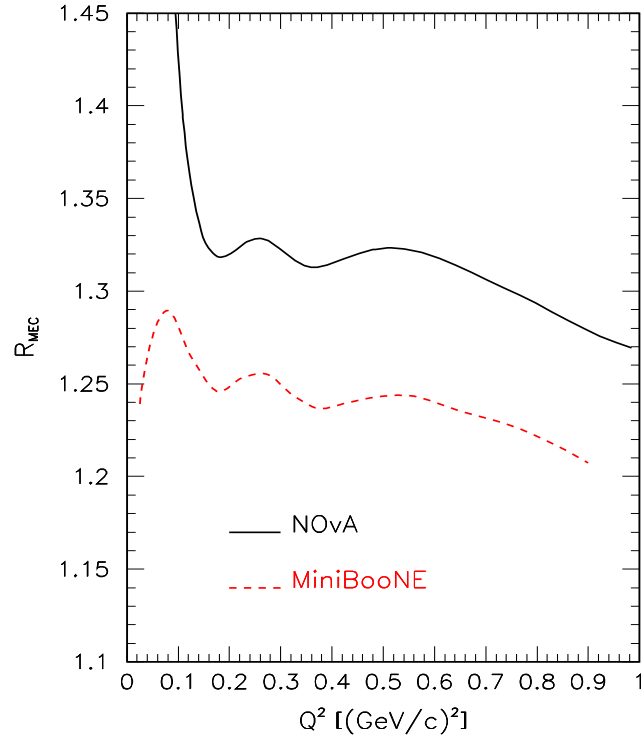


FIG. 19: The ratio R_{MEC} as a function of Q^2 for the NOvA and MiniBooNE flux-integrated $d\sigma/dQ^2$ cross sections.

and MINERvA data [46, 60]. We also extracted the values of the axial form factor $F_A(Q^2)$ as a function of Q^2 , using the measured neutrino flux-integrated $d\sigma/dQ^2$ cross section. There is a good overall agreement within the experimental uncertainties between the extracted values of $F_A(Q^2)$ and the dipole parametrization with the value of $M_A = 1.2$ GeV. We obtained that in the MiniBooNE experiment the $2p - 2h$ channel is large, contributing about 25% depending on kinematics, and it is essential to describe a great amount of experimental data. One can also notice that our calculations are in agreement with other theoretical results which are compatible with MiniBooNE data.

Using the RDWIA+MEC model with $M_A = 1.2$ GeV we estimated the differential flux-integrated CCQE-like cross sections for neutrino scattering in the NOvA near detector. We show that these cross sections are coincidence with ones for neutrino scattering on carbon. The $2p - 2h$ MEC contributions in the NOvA energy range are about of 30-35%, i.e. ~ 8 % larger than in the MiniBooNE experiment. So, the measurements of the CCQE-like differential cross sections in the NOvA experiment are necessary in order to make precision

determinations of neutrino oscillation parameters.

Acknowledgments

The authors greatly acknowledge J. Amaro and G. Megias, for fruitful discussions and for putting in our disposal the codes for calculation of the MEC's electroweak response functions that were used in this work. We specially thank A. Habig and J. Samoilova for a critical reading of the manuscript.

-
- [1] R. A. Smith and E. J. Moniz, Nucl. Phys. **B43**, 605 (1972).
 - [2] V. Bernard, L. E. Elouadrhiri, U. -G. Meissner J. Phys. **G28**, R1, (2002).
 - [3] V. Lyubushkin *et al.*, (NOMAD Collaboration), Eur. Phys. J. **C63**, 355, (2009).
 - [4] G. A. Fiorentini *et al.*, (MINERvA Collaboration), Phys. Rev. Lett. **111**, 022502 (2013).
 - [5] L. Fields *et al.*, (MINERvA Collaboration), Phys. Rev. Lett. **111**, 022501 (2013).
 - [6] L. Aliaga *et al.*, (MINERvA Collaboration), Phys. Rev. **D94**, 092005 (2016); **D95**, 039903 (2017) [Addendum]
 - [7] M. Betancour, JPS Conf. Proc. **12**, 010016 (2016)
 - [8] C. E. Patrick *et al.*, (MINERvA Collaboration), Phys. Rev. **D97**, 052002 (2018)
 - [9] A. A. Aguilar-Arevalo *et al.*, (MiniBooNE Collaboration), Phys. Rev. **D81**, 092005 (2010).
 - [10] A. A. Aguilar-Arevalo *et al.*, (MiniBooNE Collaboration), Phys. Rev. **D82**, 092005 (2010).
 - [11] A. A. Aguilar-Arevalo *et al.* (MiniBooNE Collaboration) Phys. Rev. **D88**, 032001 (2013).
 - [12] R. Gran *et al.*, (K2K Collaboration), Phys. Rev. **D74**, 052002 (2006).
 - [13] X. Espinal, F. Sanchez, AIP Conf. Proc. **967**, 117 (2007).
 - [14] P. Adamson *et al.*, (MINOS Collaboration), Phys. Rev. **D91**, 012005 (2015).
 - [15] K. Abe *et al.*, (T2K Collaboration), Phys. Rev. **D92**, 112003 (2015).
 - [16] G. T. Garvey, D. A. Harris, H. A. Tanaka, R. Tayloe, G. P. Zeller, Phys. Rept. **580**, 1 (2015).
 - [17] T. Katori, M. Martini, J. Phys. **G45**, 013001 (2018).
 - [18] L. Alvarez-Ruso *et al.*, Prog. Part. Nucl. Phys. **100**, 1 (2018)
 - [19] C. Maieron, M. C. Martinez, J. A. Caballero, and J. M. Udias, Phys. Rev. **C68**, 048501, 2003.

- [20] M. C. Martinez, P. Lava, N. Jachowicz, J. Ryckebusch, K. Vantournhout, and J. M. Udias, Phys. Rev. **C73**, 024607, 2006.
- [21] A. Meucci, C. Giusti, and F. D. Pacati, Nucl. Phys. **A739**, 277, 2004.
- [22] A. V. Butkevich and S. A. Kulagin, Phys. Rev. **C76**, 045502 (2007).
- [23] A. V. Butkevich, Phys. Rev. **C80**, 014610 (2009).
- [24] A. V. Butkevich, and D. Perevalov, Phys. Rev. **C84**, 015501 (2011).
- [25] M. Martini, M. Ericson, and G. Chanfray, Phys. Rev. **C81**, 045502 (2010).
- [26] N. Jachowicz, K. Heyde, J. Ryckebusch, and S. Rombouts, Phys. Rev. **C65**, 025501, (2002).
- [27] J. Nieves, J. E. Amaro, and M. Valverde, Phys. Rev. **C70**, 055503, (2004).
- [28] O. Benhar, N. Farina, H. Nakamura, M. Sakuda, and R. Seki, Phys. Rev. **D72**, 053005, (2004).
- [29] R. Gonzalez-Jimenez, G. D. Megias, M. B. Barbaro, J. A. Caballero, and T. W. Donnelly, Phys. Rev. **C90**, 035501 (2014).
- [30] T. Leiner, L. Alvarez-Ruso, and U. Mosel, Phys. Rev. **C73**, 065502, (2004).
- [31] A. Bodek, H. Budd, and M. Christy, Eur. Phys. J. **C71**, 1 (2011).
- [32] V. Pandey, N. Jachowicz, J. Ryckebusch, T. Van Cuyck, and W. Cosyn, Phys. Rev. **C89**, 024601 (2014).
- [33] K. Gallmeister, U. Mosel, and J. Weil. Phys. Rev. **C94**, 035502, (2016).
- [34] M. Martini, M. Ericson, and G. Chanfray, Phys. Rev. **C84**, 055502 (2011).
- [35] M. Martini, and M. Ericson, Phys. Rev. **C87**, 065501 (2013).
- [36] J. Nieves, I. Ruiz Simo, and M. J. Vicente Vacas, Phys. Lett. **B707**, 72 (2012).
- [37] J. Nieves, I. Ruiz Simo, and M. J. Vicente Vacas, Phys. Lett. **B721**, 90 (2013).
- [38] A. De Pace, M. Nardi, W. M. Alberico, T. W. Donnelly, and A. Molinari, Nucl. Phys. **A726**, 303 (2003).
- [39] I. Ruiz Simo, J. E. Amaro, M. B. Barbaro, A. De Pace, J. A. Caballero, and T. W. Donnelly, J. Phys. **G44**, 065105 (2017).
- [40] G. D. Megias, T. W. Donnelly, O. Moreno, C. F. Williamson, J. A. Caballero, R. Gonzalez-Jimenez, A. De Pace, M. B. Barbaro, W. M. Alberico, M. Nardi, and J. E. Amaro, Phys. Rev. **D91**, 073004 (2015).
- [41] G. D. Megias, J. E. Amaro, M. B. Barbaro, J. A. Caballero, T. W. Donnelly, and I. R. Simo, Phys. Rev. **D94**, 093004 (2016).
- [42] A. V. Butkevich, and S. V. Luchuk, Phys. Rev. **C97** 045502, (2018).

- [43] J. J. Kelly, Adv. Nucl. Phys. **23**, 75 (1996).
- [44] K. G. Fissum *et al.*, Phys. Rev. **C70**, 034606, 2004
- [45] J. J. Kelly, Phys. Rev. **C71**, 064610 (2005).
- [46] C. Wilkinson, R. Terri, C. Andreopoulos, A. Bercellie, C. Bronner, S. Cartwright, P. de Perio, J. Dobson, K. Duffy, A. P. Furmanski, L. Haegel, Y. Hayato, A. Kaboth, K. Mahn, K. S. McFarland, J. Nowak, A. Redij, P. Rodrigues, F. Sanchez, J. D. Schwehr, P. Sinclair, J. T. Sobczyk, P. Stamoulis, P. Stowell, R. Tacik, L. Thompson, S. Tobayama, M. O. Wascko, J. Zmuda, Phys. Rev. **D93**, 072010 (2016).
- [47] A. V. Butkevich, and D. Perevalov, Phys. Rev. **D89** 053014, (2014).
- [48] A. V. Butkevich, Phys. Rev. **C82** 055501, (2010).
- [49] NOvA Technical Design Report, FERMILAB-DESIGN-2007-01.
- [50] P. Adamson *et al.*, (NOvA Collaboration), Phys. Rev. Lett. **116**, 151806 (2016).
- [51] P. Mergell, U.-G. Meissner, and D. Drechsel, Nucl. Phys. **A596**, 367 (1996).
- [52] T. de Forest, Nucl. Phys. **A392**, 232 (1983).
- [53] B. Serot, J. Walecka, Adv. Nucl. Phys. **16**, 1 (1986).
- [54] C. J. Horowitz D. P. Murdock, and Brian D. Serot, in *Computational Nuclear Physics 1: Nuclear Structure* edited by K. Langanke, J. A. Maruhn, Steven E. Koonin (Springer-Verlag,Berlin, 1991), p.129.
- [55] D. Dutta *et al.*, Phys. Rev. **C68**, 064603 (2003).
- [56] E. D. Cooper, S. Hama, B. C. Clark, and R. L. Mercer, Phys. Rev. **C47**, 297 (1993).
- [57] C. Ciofi degli Atti and S. Simula, Phys. Rev. **C53** , 1689 (1996).
- [58] G. D. Megias and J. E. Amaro, Private communication.
- [59] G. D. Megias, J. E. Amaro, M. B. Barbaro, J. A. Caballero, T. W. Donnelly, Phys. Rev. **D94**, 013012 (2016).
- [60] C. Wilkinson, *Constraining neutrino interaction uncertainties for oscillation experiments*, Ph.D. thesis, University of Sheffield, (2015)
- [61] L. Aliaga, Ph.D. thesis, College of William and Mary, 2016, doi:10.2172/1250884
- [62] Xuebing Bu, arXiv:hep-ex/1601.01213 (2016)
- [63] G. D. Megias, M. B. Barbaro, J. A. Caballero, J. E. Amaro, T. W. Donnelly, I. Ruiz Simo, J. W Van Orden, arXiv:nucl-th/1711.00771 (2017)